Dehydra-decyclization of Tetrahydrofurans to Diene Monomers over Metal Oxides

SCHOLARONE™
Manuscripts

Dehydra-decyclization of Tetrahydrofurans to Diene Monomers over Metal Oxides

Yichen Ji[a,#], Ajibola Lawal[c,#], Andrew Nyholm[a], Raymond J. Gorte[a,b], Omar A. Abdelrahman [c,b*]

[a]Department of Chemical and Biomolecular Engineering, University of Pennsylvania, Philadelphia, PA, 19104, USA
[b]Catalysis Center for Energy Innovation, University of Delaware, 150 Academy Street, Newark, Delaware 19716, USA
[c]Department of Chemical Engineering, University of Massachusetts Amherst, 686 N. Pleasant Street, Amherst, MA, 01003, USA.

*Corresponding Author: abdel@umass.edu
# These authors contributed equally.

Abstract. The dehydra-decyclization of tetrahydrofuran (THF) to butadiene was investigated over a series of metal oxide catalysts, where a common set of chemical pathways was identified. Alongside butadiene, propene is formed via a Retro-Prins condensation as the main side product typically observed. Reaction occurred at similar temperatures on each of the oxides, but tetragonal zirconia (t-ZrO_2) and monoclinic zirconia (m-ZrO_2) were unique in showing high selectivity to butadiene (>90%). Near quantitative yields to butadiene could be achieved over t-ZrO_2 at 673 K and a WHSV of 0.93 g THF g-cat^{-1} hr^{-1}. Through contact time studies, butadiene is determined to be a primary product. Methyl-substituted THF gave only moderate increases in rates and the products showed minimal isomerization of the carbon backbone. The t-ZrO_2 catalyst was found to be relatively stable with time on stream, experiencing coking as a likely source of deactivation. Complete regeneration of the catalyst was demonstrated through calcination alone, allowing for multiple regenerations with no irreversible loss in activity or selectivity. The catalytic activity of zirconia was found to be structure insensitive, with t-ZrO_2 and m-ZrO_2 exhibiting similar initial activities; however, m-ZrO_2 was observed to deactivate much more rapidly.

1. Introduction

Conjugated 1,3 dienes serve as a vital backbone of the polymer industry. Isoprene is one of the main chemical feedstocks in car-tire manufacturing[1-3], in addition to other rubber products; butadiene is used extensively for products ranging from composite polymers, like acrylonitrile-butadiene-styrene (ABS)[4], and adiponitrile[5]. At present, these dienes are obtained primarily as a by-product of naphtha cracking for production of ethylene[6, 7]. With the recent availability of ethane from shale gas, there is no longer the need to produce ethylene from naphtha cracking[8]. Therefore, other sources of dienes are required, with "on-purpose" production technologies being highly desirable.

Recent work has demonstrated that butadiene[6], pentadienes[6, 9, 10] and hexadienes[6, 10] can be synthesized by dehydra-decyclization of cyclic ethers, including tetrahydrofuran (THF) and 2-methyltetrahydrofuran (2-MTHF). Given that 2-MTHF can be produced in reasonably high yields from pentose sugars derived from lignocellulose[11], the dienes produced in this way could also be renewable. However, despite these proof-of-concept demonstrations, improved catalysts for these reactions are required for these routes to diene synthesis be economical[12]. Processes that deliver high yields are required because, in addition to better utilization of feedstocks, this dramatically reduces the energy consumption and capital costs of downstream separation.

In past work, the best results for the selective dehydra-decyclization of cyclic ethers were achieved on solids that have Brønsted acidity. For example, Kumbhalkar et al. explored a range of materials, including amorphous silica-alumina, H-ZSM-5, H-BEA, and γ-Al$_2$O$_3$ and found that the amorphous silica-alumina catalyst showed the best performance, with yields approaching 70%[10]. Because butadiene oligomerizes readily on the strong Brønsted sites that are found on zeolites and silica-alumina, the selectivity at high conversions were most likely limited by sequential reactions of the butadiene in this work. Abdelrahman and co-workers also examined a series of Brønsted and Lewis solid acids and again reported the best performance with catalysts that were Brønsted acids[6]. Interestingly, they reported diene selectivities greater than 90% on a phosphoric-acid-infiltrated, siliceous ZSM-5 (P-SPP). The acid sites in this material are known to be very weak[13], which likely maximizes selectivity by minimizing further reaction of the butadiene product. Unfortunately, rates on the P-SPP catalyst were low, necessitating the use of prohibitively long residence times to achieve the required yields. Finally, a theoretical investigation of the cyclic-ether reactions indicated that the reaction is limited by the initial ring-opening step[14], implying that

2

increased rates for ring opening could improve the selectivity to dienes if oligomerization of products could be avoided.

In the present study, we set out to investigate other solid acids that would be capable of catalyzing the dehydra-decyclization of cyclic ethers without oligomerizing the diene products. WO_x/ZrO_2 was of interest because recent work has shown this material has Brønsted sites that are of intermediate strength between that of aluminosilicates and P-SPP[13]. Several metal oxides with Lewis acidity were also of interest because past work showed differences in their reactivity towards alcohols[15, 16]. Lewis acids would also not be expected to catalyze diene oligomerization.

While WO_x/ZrO_2 was not found to be more selective than zeolite catalysts for this reaction, the tetragonal phase of zirconia (t-ZrO_2) was found to be both active and selective for production of dienes, capable of providing yields approaching 90%. While the reaction was not structure sensitive, strong differences in the stabilities of t-ZrO_2 and monoclinic zirconia (m-ZrO_2) with time on stream were observed.

2. Materials and Methods

2.1 Material Synthesis and Characterization

A list of the catalysts that were examined in this study is given in **Table 1**, while XRD patterns for selected materials are shown in **Figure SI** of the supplementary Information. The ZrO_2 samples were prepared by dissolving zirconyl nitrate hydrate (1 g, $ZrO(NO_3)_2 \cdot xH_2O$, 99%, Sigma Aldrich in 10 mL deionized water, after which the solution was dried in oven at 333 K for 12 h and calcined in air at either 673 K for 5 h or 1173 K for 3 h to produce samples that were either primarily tetragonal or monoclinic zirconia[17]. CeO_2 and Nb_2O_5 were synthesized from cerium (III) nitrate hexahydrate ($Ce(NO_3)_3 \cdot 6H_2O$, 99.5%, ACROS organics) and niobium(V) oxalate hydrate (Alfa Aesar), respectively. 1 g of each salt was dissolved in 10 mL of deionized water and dried at 333 K for 12 h. The CeO_2 sample was then calcined at 873 K for 3 h and the Nb_2O_5 was calcined at 923 K for 3 h. TiO_2 was used as received (AEROXIDE, TiO_2, P25). The Al_2O_3 was purchased as γ-Al_2O_3 (min. 97%, Strem Chemicals), but was calcined at 1173 K for 24 h before use. NH_4-ZSM-5 was purchased from Zeolyst International (CBV5524G, Si/Al=25 and CBV28014, Si/Al=140) and converted to H-ZSM-5 by calcination in flowing air at 823 K for 6 hours. No significant difference in selectivity was observed with the choice of different ZSM-5 zeolites.

The WO_x/ZrO_2 was prepared by Atomic Layer Deposition (ALD), using procedures identical to that used in a previous study[18]. The ZrO_2 in this case was a mixture of tetragonal and monoclinic phases and was prepared by precipitation of an aqueous solution of $ZrO(NO_3)_2 \cdot xH_2O$ using ammonia. ALD was performed in a static system using $W(CO)_6$ and O_2 as the precursor and oxidant, respectively. Samples with varying WO_x loadings were tested for the dehydra-decyclization of THF; however, since the results for all WO_x/ZrO_2 samples were similar, only those results for the sample with 5 ALD cycles (5R WO_x/ZrO_2, WO_x loading of 10.1-wt%) will be reported. Of the WO_x/ZrO_2 catalysts prepared by ALD, the sample with 5 ALD cycles had the maximum Brønsted site concentration, 80 µmol/g as measured by temperature programmed desorption/thermogravimetric Analysis (TPD-TGA) of 2-propanamine[18].

X-ray diffraction (XRD) patterns for the various samples were measured on a Rigaku MiniFlex diffractometer equipped with a Cu Kα source (λ = 154.05 pm). BET measurements were performed using N_2 at 78 K on a home-built adsorption system. TPD-TGA measurements were carried out in vacuum on 50-mg samples placed in the sample pan of a CAHN 2000 microbalance[19]. After heating the sample in 10^{-7} Torr to 823 K, the sample was cooled to room temperature, exposed to ~10 Torr of vapor from the adsorbate of interest, and then evacuated for 1 h. Desorption measurements were performed by heating the sample at 10 K/min while measuring the partial pressures with an SRI quadrupole mass spectrometer (RGA100).

2.2 Catalytic Testing

Catalyst testing was performed in two similar, fixed-bed reactors at the University of Massachusetts Amherst and the University of Pennsylvania. Samples, ~200 mg in size, were placed in the center of ¼-in, tubular reactors and held in place with glass wool. All reaction experiments were performed at atmospheric pressure. Prior to measuring conversions, the catalyst samples were calcined *in situ* at 673 K in flowing air. Liquid reactants were introduced into a flowing stream of He using a syringe pump (PHD 2000 Infusion, Harvard Apparatus). On-line analysis of the reactor effluents was performed with either a gas chromatograph (Agilent 7890B), equipped with a quantitative carbon detector (Polyarc[TM], QCD[20]) and a flame ionization detector (FID), using an HP-PLOT Q column (Agilent, 19091P-QO4), or with a GC-Mass Spec (QP5000, Shimadzu), using a capillary column (HP-INNOWAX, Agilent Technologies). Carbon balances closed to within ±10% for all reported measurements. Reactants were purchased and used without

further treatment: tetrahydrofuran (≥99.9%, Sigma Aldrich), 2-methyltetrahydrofuran (≥99%, Sigma Aldrich) and 2,5-dimethyltetrahydrofuran (≥96%, mixture of *cis-* and *trans-*, Sigma Aldrich).

Microcatalytic screening was carried out in a reactor setup previously described[6, 9]. Briefly, the catalyst was placed within a gas chromatograph (GC) quartz inlet liner, where the GC can then control the temperature of the catalyst. Furan pulses were introduced to the catalyst bed using an automated liquid sampler, injecting 1.0 µL liquid of the desired furan at a rate of 1.0 µL min^{-1}. The injected liquid contacted deactivated quartz wool placed above the catalyst bed where the liquid evaporated and was carried by a He carrier stream over the catalyst bed; the resulting products then exited the GC inlet liner and entered the GC column/detector for separation and quantification.

3. Results & Discussion

Over the various solid-acid catalysts investigated, the main carbon containing products observed were butadiene, propene, butene and butanal (**Figure 1**). All four product groups are proposed to share a common reaction intermediate: a ring-opened THF species stabilized on the catalyst surface[10, 14]. Once the ring-opened THF species is formed, it can then diverge in chemical pathways to reach the four main product groups. The intermediate can undergo dehydration to produce the desired product of butadiene. Alternatively, an equimolar amount of propene and formaldehyde can form through a Retro-Prins condensation pathway. Keto-enol tautomerization of the ring opened THF species leads to the formation of butanal, which can then undergo self-aldol condensation to form larger hydrogen-donor species[21, 22]. These hydrogen-donors are then proposed to reduce butadiene, leading to the formation of the observed butene(s) product[21].

3.1 Initial Catalyst Screening

An initial evaluation of each catalyst in **Table 1** was performed by measuring the conversion and product selectivities as a function of temperature at a fixed THF partial pressure (P_{THF} = 38 Torr), maintaining a constant weight-hourly space velocity (WHSV = 0.93 g THF g-cat^{-1} hr^{-1}, **Figure 2**). To minimize the effect of catalyst deactivation, reactor temperatures were ramped rapidly (25 K min^{-1}) to the indicated measurement condition, so that measurements over the entire temperature range could be made in approximately 2 hours. At each temperature, the conversion and product distributions were measured twice, with the results in **Figure 2** showing

the average of the two measurements. Although some catalyst deactivation occurred at the higher temperatures, there was no evidence that selectivity was severely affected by deactivation, as evidenced by the fact that results from sequential measurements were nearly identical (See the supplementary information, **Table SI**).

Results for the two catalysts that had significant Brønsted acidity, H-ZSM-5 and 5R WO_x/ZrO_2, are shown in **Figure 2A** and **2B**. H-ZSM-5 was considerably more active, exhibiting a conversion approaching 100% at 673 K, while the conversion on 5R WO_x/ZrO_2 was less than 50% at that temperature. This is partly due to the weaker Brønsted acidity of 5R WO_x/ZrO_2, indicated by the 100 K higher onset-of-reaction temperature on 5R WO_x/ZrO_2 relative to H-ZSM-5. The significantly larger Brønsted acid site density of H-ZSM-5 (420 µmol/g on H-ZSM-5 versus 80 µmol/g on 5R WO_x/ZrO_2) also affects the difference in observed activity. 5R WO_x/ZrO_2 was found to be more selective to butadiene than H-ZSM-5 across all conditions, with maximum selectivities of 45% at 623 K (5R WO_x/ZrO_2) and 35% at 523 K (H-ZSM-5). The major side products observed for both catalysts were propene, butene and butanal. The formation of propene, together with CO_2 that likely forms by decomposition of formaldehyde, indicated that Retro-Prins condensation was a major side reaction.

The results for $t-ZrO_2$ and $m-ZrO_2$, **Figure 2C** and **2D**, are significantly more interesting. On both samples, conversions were negligible below 573 K; however, above this temperature, the selectivity to butadiene was greater than 80%. Conversions were significantly higher on $t-ZrO_2$, possibly due to its higher surface area (84 $m^2 g^{-1}$ tetragonal vs. 20 $m^2 g^{-1}$ monoclinic). The high selectivity to butadiene was maintained under all reaction conditions tested, even at elevated conversions and temperatures. At 723 K, the yield to butadiene over $t-ZrO_2$ was approximately 80% in this initial screening. The major side products were propene and butene.

Results on the other oxides were less promising. $\gamma-Al_2O_3$ was found to be a relatively active catalyst, but with limited selectivity to butadiene (<15%, **Figure 2E**). TiO_2 was reasonably selective to butadiene (~40%), more so than either H-ZSM-5 or 5R WO_x/ZrO_2; but butene and propene were still major side products (**Figure 2F**). CeO_2 also showed reasonable selectivity at 673 K (~60%, **Figure 2G**), but butene and propene were still formed in significant concentrations. THF conversions on Nb_2O_5 were much lower (**Figure 2H**), due at least in part to its lower surface area, making the comparison to the other oxides difficult. However, it is worth noting that the surface area of the Nb_2O_5 sample was only a factor of two lower than that of $m-ZrO_2$, for which

the conversion and selectivity were both significantly larger. Nevertheless, the selectivity to butadiene over Nb_2O_5 was found to be relatively limited (~ 40%).

Overall, the following trend for selectivity to butadiene was established (**Figure 3**):

$$t\text{-}ZrO_2 \approx m\text{-}ZrO_2 \gg CeO_2 > Nb_2O_5 \approx TiO_2 > 5R \; WO_x/ZrO_2 > H\text{-}ZSM\text{-}5 > \gamma\text{-}Al_2O_3$$

Clearly, the two Brønsted acids in this group of materials were not selective but the trend among Brønsted acids tested suggests that weaker acids are better, with P-SPP > 5R WO_x/ZrO_2 > H-ZSM-5[13]. Lewis-acid strength is much more difficult to define or measure; however, if one takes the TPD peak temperature for the 2-propanol dehydration reaction as a measure of Lewis-acid strength, there appears to be a trend between selectivity and Lewis-acid strength. TPD-TGA data for 2-propanol are shown in **Figure SII** of the Supplementary Information and propene peak desorption temperatures are listed in **Table SII**. Based on these values, the two zirconia samples are the weakest of the solid acids as well as the most selective, followed by CeO_2. Obviously, the properties of ZrO_2 and CeO_2 cannot all be explained in terms of Lewis acidity but the correlation between 2-propanol dehydration temperatures and butadiene selectivities is still intriguing. It also is interesting to notice that alcohol dehydration[23-25] and alkene-aldehyde Prins condensation[26-28], two chemistries strongly related to dehydra-decyclization, are also strongly affected by the strength of the solid acid.

3.2 TPD-TGA Measurements

In order to gain insights into the reactions, TPD-TGA measurements were performed for THF on the samples in **Table 1**. Results for the two Brønsted-acid catalysts are shown in **Figure 4**, while those for two representative Lewis acids, t-ZrO_2 and TiO_2, are shown in **Figure 5**. Data for other solid acids from **Table 1** are reported in **Figure SIII** of the supplementary information. A comparison between H-ZSM-5 and 5R WO_x/ZrO_2 in **Figure 4** demonstrates clear differences between these materials. The TPD-TGA results for THF on H-ZSM-5, **Figure 4A**, shows that some unreacted THF desorbed intact at lower temperatures but significant product desorption was observed starting at 450 K. We have not shown the water desorption curves because they occurred over a wide temperature range on the oxide samples, as discussed elsewhere [29]. It is also not easy to identify hydrocarbon products from the mass spectra but simultaneous evolution of products with peaks at m/e = 41, 54, and 56 suggest that a complex mixture of hydrocarbons is formed. Given that the primary products from the reaction of THF are expected to oligomerize rapidly[30], the desorbing species are likely formed by cracking of these oligomers. A further observation of a

series of peaks represented by m/e = 67 at 600 K also suggests formation of oligomers on the strongly Brønsted acidic H-ZSM-5. Results for 5R WO_x/ZrO_2 (**Figure 4B**) are significantly simpler. Starting from an initial coverage of ~70 μmol/g (7.3×10^{17} molecules/m^2), about half of the THF desorbed intact at lower temperatures, while the rest desorbed as a product in a relatively sharp peak centered at 520 K. The fact that this product had a major peak at m/e = 54, with no peaks at either m/e = 41 or 56, implies that the product was almost pure butadiene. Given the simple product slate, it is surprising that 5R WO_x/ZrO_2 was not a selective catalyst for the steady-state reaction. However, the disappearance of product peaks around 520 K and 600 K on 5R WO_x/ZrO_2 compared to H-ZSM-5 indicates oligomerization is less likely to happen on a weaker Brønsted acid[13, 30]. This is consistent with the observation that strong Brønsted acids are not selective for THF dehydra-decyclization.

The comparison of the two representative Lewis acids, TiO_2 and t-ZrO_2, in **Figure 5** is also of interest. The initial coverage of THF after evacuation was approximately 1×10^{18} molecules/m^2 on both samples and about half of this again desorbed unreacted below 500 K. With TiO_2, desorption curves (**Figure 5A**) were similar what was observed on 5R WO_x/ZrO_2, with most of the product leaving the sample as butadiene (m/e = 54) in a peak at 600 K. A small amount of propene (m/e = 41) was also formed simultaneously. On t-ZrO_2, the products formed above 500 K were different (**Figure 5B**). Large amounts of propene and H_2 (m/e =2) desorbed almost simultaneously with the butadiene around 600 K, with additional H_2 and CO_2 (m/e =44) leaving the sample above 650 K. A review of the results in **Figure 5** and **Figure SIII** shows that t-ZrO_2 and m-ZrO_2 were unique among the oxides in showing the formation of H_2 and propene desorbing with the butadiene and in showing CO_2 and H_2 forming at higher temperatures. A plausible explanation is that H_2 and CO_2 are formed via the decomposition of formaldehyde, a product of the Retro-Prins condensation ($C_4H_8O \rightarrow C_3H_6+CH_2O$). Formaldehyde readily decomposes to H_2 and CO even at room temperature and could be responsible for the H_2 peak observed around 600 K. Because zirconia may be somewhat reducible[31], CO_2 may form by reaction of CO, forming carbonates, bicarbonates or even formates which decompose above 650 K [32-34].

3.3 Dehydra-decyclization of Methyl Substituted Furans

It seems likely that the reaction intermediates on Lewis-acid catalysts differ significantly from those which are formed on Brønsted acids. Over purely Brønsted acidic catalysts, a carbocation mechanism has been invoked to explain the dehydra-decyclization chemistry[14]. This

is consistent with the rate of ring opening acting as a dominant rate-determining step, involving the formation of a carbocation species at the 2 or 5 ring position. To gauge whether this mechanism holds true over ZrO_2, we measured the rate of diene formation over cyclic ethers with varying degrees of methyl-substitution (THF, 2-MTHF and 2,5-DMTHF). The more stable tertiary carbocation formed from 2,5-DMTHF will lead to an increased rate of diene formation relative to the secondary carbocation of THF. Over H-ZSM-5, we find that the rate of diene formation significantly increases with methyl substitution (**Figure 6**). Relative to the rate of THF dehydra-decyclization, the rate of 2-MTHF and 2,5 DMTHF is 8 and 20 times larger, respectively. Similarly, over an H-ZSM-5 catalyst (Si/Al = 140), Dauenhauer et. al recently reported that only methyl substitution at the 2 and 5 carbon position leads to an increase in the rate of diene formation[35]. Dumesic et. al also reported a similar result over amorphous silica alumina, where tetrahydrofuran and tetrahydropyran (THP) were also found to be comparable in activity[10]. While the same qualitative trend is observed over ZrO_2 (2,5-DMTHF > 2-MTHF > THF), the relative rate enhancement with increasing methyl substitution is significantly reduced. For example, the rate of diene formation from 2,5-DMTHF over ZrO_2 is 7 times faster than from THF. This is significantly smaller than the factor of 20 experienced over Brønsted acidic catalysts. Similarly, when comparing the relative rates of 2-MTHF and 2,5-DMTHF, a marginal change is experienced with ZrO_2 compared with the large increase (2-3 times) over H-ZSM-5. This suggests that, while a carbocation mechanism could also be relevant to dehydra-decyclization over ZrO_2, it is not as kinetically relevant as with purely Brønsted acidic catalysts like H-ZSM-5.

The difference in the nature of dehydra-decyclization over the two catalysts is also apparent when considering the extent of diene isomerization. While aluminosilicates are moderately selective to pentadienes from 2-MTHF[6, 10], the ratio of 1,3 to 1,4 pentadiene selectivity ($S_{1,3}/S_{1,4}$) is approximately equal to two across a range of operating conditions. Conversely, t-ZrO_2 shows a ratio of ~ 26 at 673 K that is stable with time on stream (supplementary information, **Figure SIV**). This order of magnitude difference in the relative selectivity of 1,3 and 1,4 pentadiene demonstrates the lack of isomerization over zirconia, again suggesting a reduced carbocation character relative to aluminosilicates. Even with weaker Brønsted acids, like all-silica phosphorous containing zeolites (P-SPP), a relatively low ratio of ~ 4 is observed[6].

3.4 Catalytic Stability of ZrO_2

In addition to ZrO_2 being an active and selective catalyst for the dehydra-decyclization of THF, it is necessary that it be able to maintain its desirable catalytic performance under reaction conditions. To this end, we examined the catalytic stability of ZrO_2 by monitoring the activity of the catalyst for 10 hours on stream at 673 K. Given the difference in specific surface areas (**Table 1**), catalyst masses of 0.2 and 0.8 g were used for t-ZrO_2 and m-ZrO_2, respectively, to ensure measurements were performed with the same total catalyst surface area. It is worth noting that the selectivity to butadiene, propene and butene over t-ZrO_2 did not vary with WHSV, indicating that they are all primary products (**Supplementary information, Figure SV**).

An earlier comparison of the two phases of zirconia at 673 K showed that t-ZrO_2 is more active, as indicated by a larger conversion on a mass normalized basis (fixed WHSV, **Figure 3**); the initial conversions of THF were nearly 100% on both phases at this temperature. Both zirconia catalysts were significantly more active than the most selective P-SPP catalyst previously identified. That catalyst showed 83% conversion and a butadiene selectivity of 87% at 673 K with a WHSV of 0.04 g THF g-cat^{-1} hr^{-1} with [6]. A similar conversion was achieved on both zirconia samples at a WHSV more than an order of magnitude higher (0.93 g THF g-cat^{-1} hr^{-1}). Despite the increased activity with zirconia, the selectivity to butadiene was comparable on both catalysts.

Significant deactivation was observed on both zirconia phases after 10 hours on stream (**Figure 7A**). THF conversion decreased to ~ 60% and 20% on tetragonal and monoclinic zirconia, respectively. m-ZrO_2 also exhibited a rapid drop in conversion during the first 2 hours on-stream, while the conversion decayed in a steady manner on t-ZrO_2. The selectivity to butadiene on both catalysts remained unchanged as a function of deactivation (**Figure 7B**). This suggests that the mode of deactivation leads to a reduction in the number of available active sites, rather than a change in their nature. Given the presence of hydrocarbons over a solid acid at moderately high temperatures, deactivation is likely due to coking, to which tetragonal zirconia appears to be more resistant.

We investigated whether the catalytic activity could be restored by removing possible carbonaceous deposits. First the catalysts were regenerated through an in-situ calcination at 673 K (**Figure 8**). The catalyst activity was found to be completely restored following this treatment, consistent with the proposed coking deactivation mechanism. The activity profile for the regenerated catalyst with time on stream was also found to be identical to that of the fresh catalyst,

even after multiple regenerations. Regeneration of m-ZrO_2 showed identical results, with the catalytic activity again restored and an identical deactivation profile observed after regeneration (**Supplementary information, Figure SVI**).

To quantify the surface concentration of deactivating surface species, the spent catalysts were calcined in flowing oxygen while measuring the moles of CO_2 evolved. Each catalyst was first exposed to conditions identical to those of **Figure 7** (673 K, P_{THF} = 38 torr, WHSV = 0.93 g THF g-cat^{-1} hr^{-1}) for 10 hours on stream, then transferred to another flow reactor equipped with an on-line mass spectrometer. Prior to calcination, the catalyst was exposed to 20 sccm of He for 1 hour at 673 K to remove any light residual adsorbates. The catalysts were then calcined at 873 K in a 1 sccm stream of pure oxygen, after which the catalyst was collected and weighed to confirm no significant loss in mass relative to the fresh catalyst. The total amounts of CO_2 that evolved during calcination of the ZrO_2 catalysts is shown in **Table 2**, 220 μmol g-cat^{-1} for t-ZrO_2 and 150 μmol g-cat^{-1} for m-ZrO_2. If we assume that the entire carbon loss under reaction conditions turned into condensed organics (detected as CO_2, **Table 2**), the carbon balances on both t-ZrO_2 and m-ZrO_2 would still be greater than 99%. Comparing the amount of CO_2 per surface area of catalyst, t-ZrO_2 appears to be more resistant to coking than m-ZrO_2, with 2.6 μmol CO_2 m^{-2} and 7.5 μmol CO_2 m^{-2}, respectively. This conclusion is consistent with the more stable activity profile of t-ZrO_2 with time on stream (**Figure 7A**).

3.5 CO_x as deactivating species

It has been reported that CO and CO_2 adsorb on zirconia by forming surface carbonates[32, 33] and that high temperatures are required to desorb and regenerate the original zirconia surface. In our reaction, CO_2 has been observed as a side product while CO is potentially formed from the decomposition of formaldehyde. We therefore investigated the possibility that deactivation is due to carbonate formation by measuring the adsorption of CO_2 on the ZrO_2 catalysts at relevant reaction conditions. Both catalysts were pretreated in 20 sccm He at 673K for 30 min to remove water. After this pretreatment, the flow was switched to a 20 sccm stream of pure CO_2 until the point of saturation, then switched back to He followed by heating to 873 K at a rate of 10 K min^{-1}. The amount of adsorbed CO_2 per unit surface area on t-ZrO_2 is also lower than that on m-ZrO_2, with values of 0.6 μmol m^{-2} and 1.0 μmol m^{-2}, respectively (**Table 2**). However, both of these values are significantly lower than the amount of CO_2 that evolved from the deactivated catalysts

during calcination. Therefore, CO_2 adsorption on ZrO_2 likely plays only a very minor role in deactivation compared to hydrocarbon coking.

3.6 Apparent Energetics of Dehydra-decyclization on ZrO₂

To further confirm the structure insensitive nature of dehydra-decyclization on ZrO_2, we measured the apparent activation energy of dehydra-decyclization over both catalysts. Utilizing a pulsed microreactor, in which small amounts of THF (1 µL, 12.4 µmol) were individually introduced, the catalytic behavior of the two phases could be compared in the absence of significant deactivation. At 673 K, both achieved nearly identical selectivities to butadiene (95% monoclinic, 97% tetragonal) at non-trivial THF conversion levels (> 10%). Furthermore, we found the apparent activation energies of the reactions on the two phases over a the temperature range of 573 to 673 K to be statistically indistinguishable. The apparent activation energies for butadiene formation from THF were measured to be 15.6 ± 2.9 and 17.8 ± 0.8 kcal mol^{-1} over tetragonal and monoclinic ZrO_2, respectively (**Figure 9**). While the activity of the two phases is different, this difference cannot be attributed to the nature of the active sites. This is further underscored by the relatively fixed ratio of rates for butadiene formation over the two phases ($r_{tetragonal}/r_{monoclinic} \sim 2.5$), which are likely explained by a difference in the active site density of the two phases, leading to a fixed ratio of rates and identical activation energies. Therefore, we suggest that there are no intrinsic differences in the nature of the active site for the two phases; $m\text{-}ZrO_2$ is simply more susceptible to deactivation via coking.

4. Conclusion

The dehydra-decyclization of THF and other methyl substituted furans were investigated over metal oxides. While previous reports have focused on the use of Brønsted acidic catalysts, we demonstrate here the utility of oxides with Lewis acidity. High selectivity to butadiene from THF is achieved over a bulk ZrO_2 catalyst (> 90%), with near quantitative yields at reasonable weight hourly space velocities (~1 g THF g-cat^{-1} h^{-1}). Preliminary mechanistic investigations of ZrO_2 suggest that product distributions are similar to what is reported for purely Brønsted acidic materials, like H-ZSM-5; however, the energetics for the reaction are significantly different and warrant further investigation. Monoclinic zirconia is found to deactivate much more rapidly compared to tetragonal zirconia, even though the two phases exhibit similar initial activities. Deactivation occurs due to coking, but is completely reversible by simple calcination. Ultimately,

we have demonstrated that the commonly employed catalyst support material, ZrO_2, can act as an effective catalyst in of itself for a complex chemistry.

Conflicts of Interest
There are no conflicts to declare.

Acknowledgements

References

1. K. Rose and A. Steinbuchel, *Appl. Environ. Microbiol.*, 2005, **71**, 2803-2812.
2. K. Stevenson, B. Stallwood and A. G. Hart, *Bioremediat. J.*, 2008, **12**, 1-11.
3. A. R. C. Morais, S. Dworakowska, A. Reis, L. Gouveia, C. T. Matos, D. Bogdał and R. Bogel-Łukasik, *Catal. Today*, 2015, **239**, 38-43.
4. S. Olivera, H. B. Muralidhara, K. Venkatesh, K. Gopalakrishna and C. S. Vivek, *J. Mat. Sci.*, 2016, **51**, 3657-3674.
5. D. E. Blanco, A. Z. Dookhith and M. A. Modestino, *React. Chem. Eng.*, 2019, **4**, 8-16.
6. O. A. Abdelrahman, D. S. Park, K. P. Vinter, C. S. Spanjers, L. Ren, H. J. Cho, D. G. Vlachos, W. Fan, M. Tsapatsis and P. J. Dauenhauer, *ACS Sus. Chem. Eng.*, 2017, **5**, 3732-3736.
7. E. V. Makshina, M. Dusselier, W. Janssens, J. Degreve, P. A. Jacobs and B. F. Sels, *Chem. Soc. Rev.*, 2014, **43**, 7917-7953.
8. Y. Xiang, H. Wang, J. Cheng and J. Matsubu, *Catal. Sci. Tech.*, 2018, **8**, 1500-1516.
9. O. A. Abdelrahman, D. S. Park, K. P. Vinter, C. S. Spanjers, L. Ren, H. J. Cho, K. Zhang, W. Fan, M. Tsapatsis and P. J. Dauenhauer, *ACS Catal.*, 2017, **7**, 1428-1431.
10. M. D. Kumbhalkar, J. S. Buchanan, G. W. Huber and J. A. Dumesic, *ACS Catal.*, 2017, **7**, 5248-5256.
11. *United States Pat.,* 5883266, 1999.
12. D. J. Lundberg, D. J. Lundberg, K. Zhang and P. J. Dauenhauer, *ACS Sus. Chem. Eng.*, 2019, **7**, 5576-5586.
13. C. Wang, S. Li, X. Mao, S. Caratzoulas and R. J. Gorte, *Catal. Lett.*, 2018, **148**, 3548-3556.
14. S. Li, O. A. Abdelrahman, G. Kumar, M. Tsapatsis, D. G. Vlachos, S. Caratzoulas and P. J. Dauenhauer, *ACS Catal.*, 2019, **9**, 10279-10293.
15. D. Sun, S. Arai, H. Duan, Y. Yamada and S. Sato, *Appl. Catal., A*, 2017, **531**, 21-28.
16. Y. Wang, D. Sun, Y. Yamada and S. Sato, *Appl. Catal., A*, 2018, **562**, 11-18.
17. Y. C. Zhang, S. Davison, R. Brusasco, Y. T. Qian, K. Dwight and A. World, *J. Less Common Met.*, 1986, **116**, 301-306.
18. C. Wang, X. Mao, J. Lee, T. Onn, Y.-H. Yeh, C. Murray and R. Gorte, *Catal.*, 2018, **8**, 292-306.

19.   Y.-H. Yeh, R. J. Gorte, S. Rangarajan and M. Mavrikakis, *J. Phys. Chem., C*, 2016, **120**, 12132-12138.
20.   S. Maduskar, A. R. Teixeira, A. D. Paulsen, C. Krumm, T. J. Mountziaris, W. Fan and P. J. Dauenhauer, *Lab Chip*, 2015, **15**, 440-447.
21.   F. Lin and Y.-H. C. Chin, *ACS Catal.*, 2016, **6**, 6634-6650.
22.   Y. Yang, F. Lin, H. Tran and Y.-H. C. Chin, *ChemCatChem*, 2017, **9**, 287-299.
23.   S. Hočevar, J. Batista and V. Kaučič, *J. Catal.*, 1993, **139**, 351-361.
24.   D. M. Sung, Y. H. Kim, E. D. Park and J. E. Yie, *Res. Chem. Intermed.*, 2010, **36**, 653-660.
25.   R. T. Carr, M. Neurock and E. Iglesia, *J. Catal.*, 2011, **278**, 78-93.
26.   E. Dumitriu, V. Hulea, I. Fechete, C. Catrinescu, A. Auroux, J.-F. Lacaze and J.-F. Lacaze, *Appl. Catal., A*, 1999, **181**, 15-28.
27.   E. Dumitriu, T.-O. Do and S. Kaliaguine, *J. Catal.*, 1997, **170**, 150-160.
28.   S. Wang and E. Iglesia, *ACS Catal.*, 2016, **6**, 7664-7684.
29.   C. Lin, A. C. Foucher, Y. Ji, C. D. Curran, E. A. Stach, S. McIntosh and R. J. Gorte, *ACS Catal.*, 2019, **9**, 7318-7327.
30.   O. Kresnawahjuesa, *J. Catal.*, 2002, **210**, 106-115.
31.   S. Sharma, S. Hilaire, J. M. Vohs, R. J. Gorte and H. W. Jen, *J. Catal.*, 2000, **190**, 199-204.
32.   K. Pokrovski, K. T. Jung and A. T. Bell, *Langmuir*, 2001, **17**, 4297-4303.
33.   K. T. Jung and A. T. Bell, *Catal. Lett.*, 2002, **80**, 63-68.
34.   E. I. Kauppi, K. Honkala, A. O. I. Krause, J. M. Kanervo and L. Lefferts, *Top. Catal.*, 2016, **59**, 823-832.
35.   G. Kumar, D. Liu, D. Xu, L. Ren, M. Tsapatsis and P. J. Dauenhauer, *Green Chem.*, 2020, DOI: 10.1039/d0gc00136h.
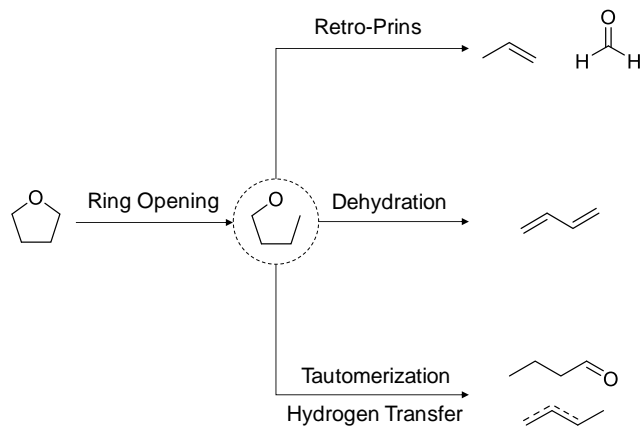
Figure 1: **Overall chemical pathways to the various products observed (Butadiene, Propene, Butene and Butanal), proceeding through a proposed ring opened intermediate.**
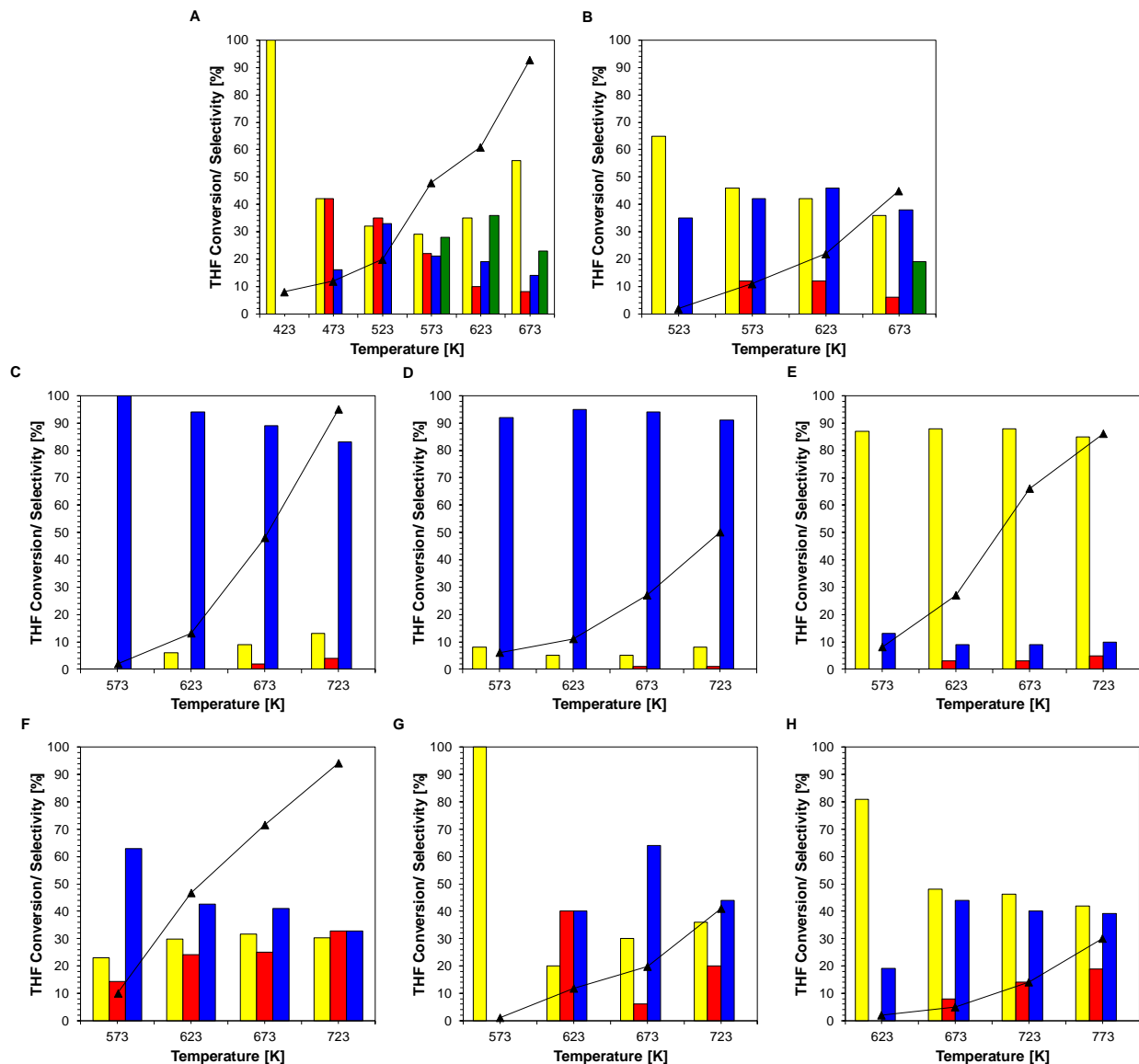
Figure 2. Catalytic screening of tetrahydrofuran dehydra-decyclization from 423 ~ 773 K, at 38 Torr THF and WHSV of 0.93 g THF g-cat^{-1} hr^{-1}. A. H-ZSM-5 **B.** 5R WO$_x$/ZrO$_2$ **C.** t-ZrO$_2$ **D.** m-ZrO$_2$ **E.** Al$_2$O$_3$ **F.** TiO$_2$ **G.** CeO$_2$ **H.** Nb$_2$O$_5$. (THF conversion: ▲, product selectivity is represented by bars with different colors, i.e. yellow: **propene**, red: **butene(s)**, blue: **butadiene**, green: **butanal**.)

Catalysis Science & Technology
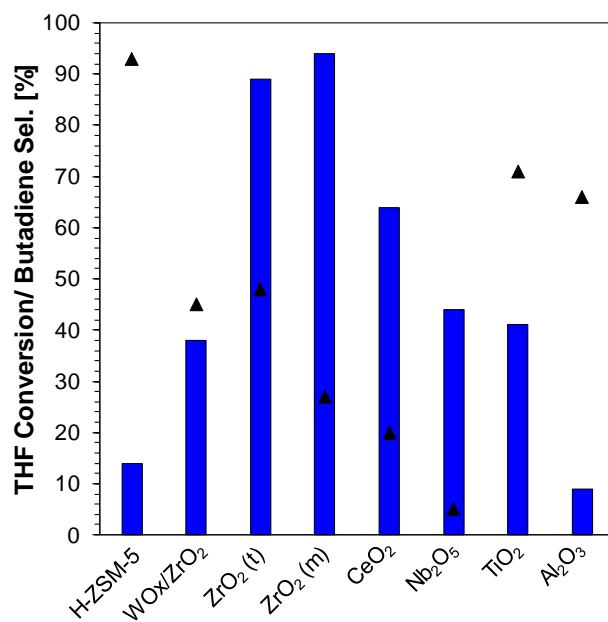
Figure 3. THF conversion and selectivity to butadiene on different catalysts at 673 K, 38 Torr THF and WHSV of 0.93 g THF g-cat^{-1} hr^{-1}. THF conversion: ▲, selectivity to butadiene: blue bar.
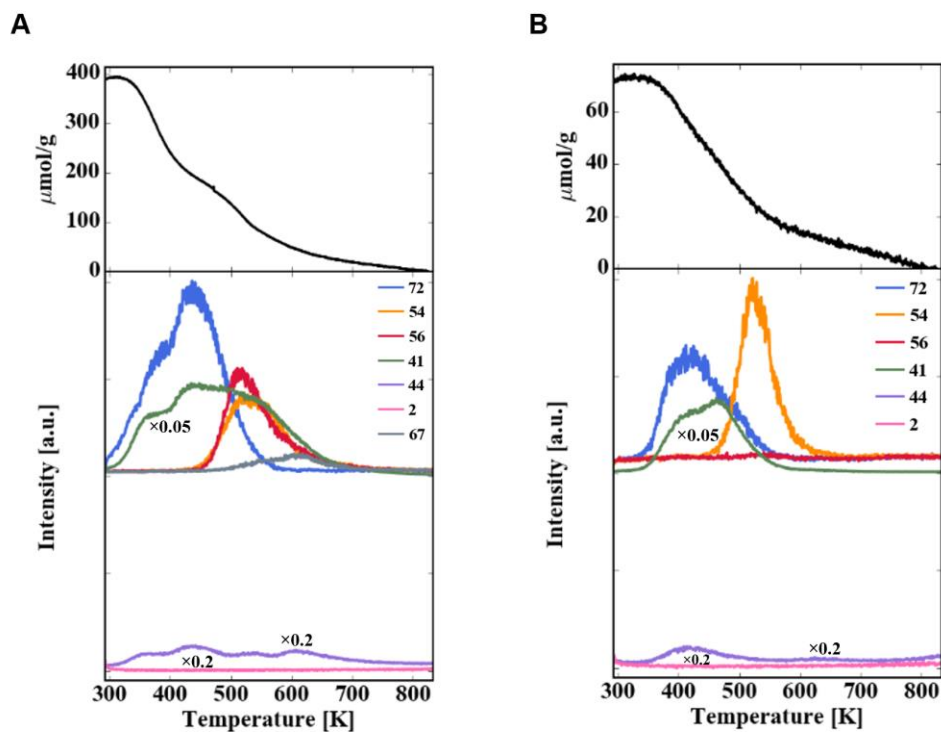
Figure 4. Temperature Programmed Desorption - Thermogravimetric Analysis of THF on A. H-ZSM-5 **B.** 5R WO_x/ZrO_2. The TPD peaks correspond to THF (m/e = 72,41), butadiene (m/e = 54), butene (m/e = 56), propene (m/e = 41), CO_2 (m/e = 44), H_2 (m/e = 2), oligomer cracking species (m/e = 41, 54, 56, 67).
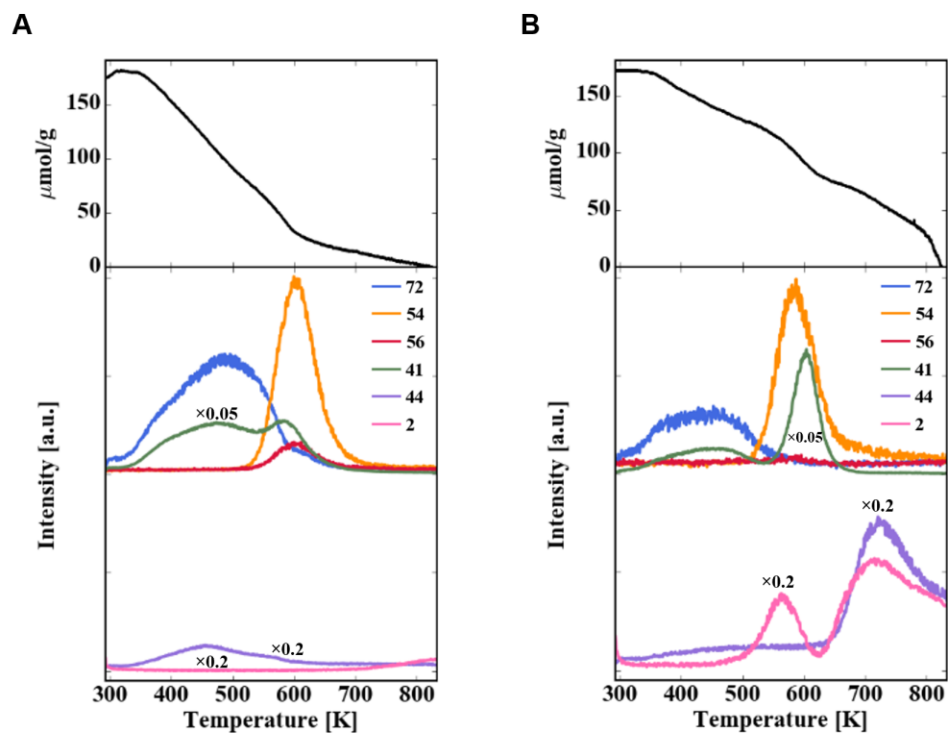
Figure 5. Temperature Programmed Desorption - Thermogravimetric Analysis of THF on A. TiO_2 **B.** t-ZrO_2. The TPD peaks correspond to THF (m/e = 72,41), butadiene (m/e = 54), butene (m/e = 56), propene (m/e = 41), CO_2 (m/e = 44), H_2 (m/e = 2).
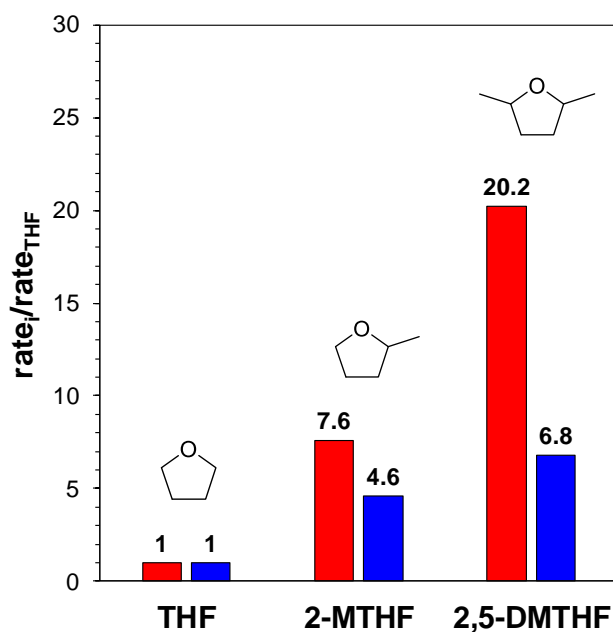
Figure 6. Comparison of relative rate of dehydra-decyclization of THF, 2-MTHF and 2,5-DMTHF over H-ZSM-5 (red) and ZrO₂ (blue) at 523 K. The reaction rate on each catalyst is normalized by the rate of THF dehydra-decyclization.
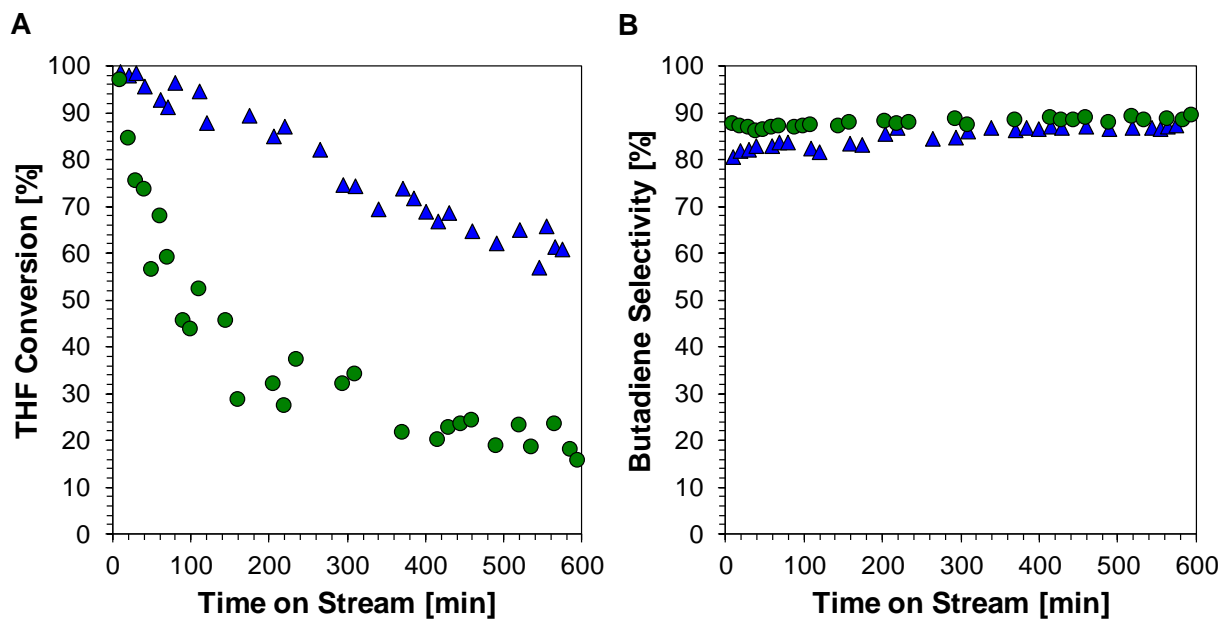
Figure 7. Dehydra-decyclization of THF on tetragonal (▲) and monoclinic (●) ZrO₂ at 673 K, 38 Torr THF and WHSV of 0.93 and 0.23 g THF g-cat^{-1} hr^{-1} for t-ZrO₂ and m-ZrO₂, respectively (0.01 g THF m^{-2} ZrO₂ hr^{-1}) A. THF conversion with time on stream **B.** Selectivity to butadiene with time on stream.

A

B
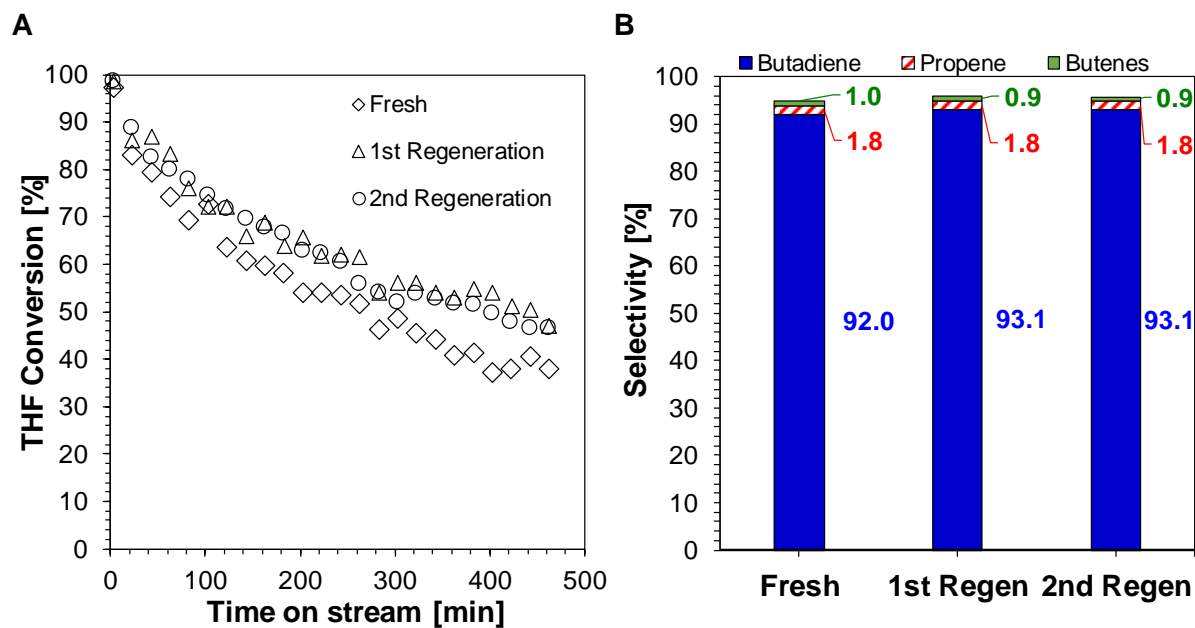
Figure 8. Dehydra-decyclization of THF on tetragonal ZrO$_2$ at 673 K, P$_{THF}$ = 10 Torr and WHSV = 0.6 g THF g-cat^{-1} hr^{-1} A. Conversion of THF with time on stream on a fresh sample of ZrO$_2$, followed by multiple calcinations at 673 K to regenerate the catalyst **B.** Selectivity to Butadiene, Propene and Butene over fresh and regenerated catalysts. Product selectivity did not vary with time on stream.

Catalysis Science & Technology
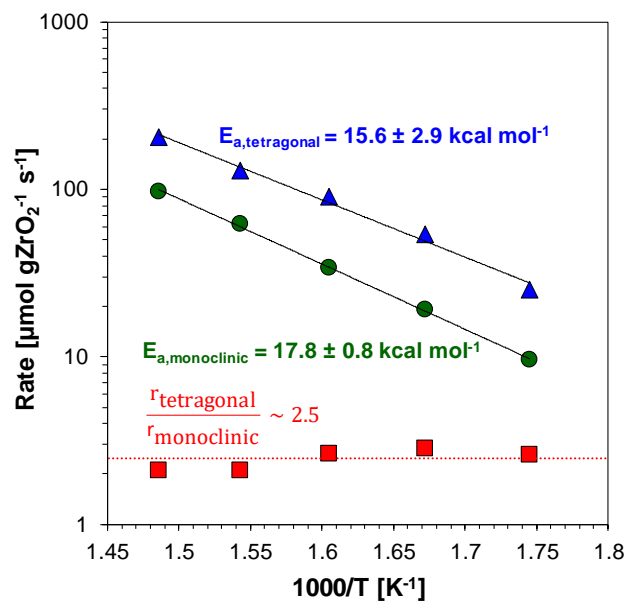
Figure 9. Comparison of activation energies between monoclinic (●) and tetragonal (▲) ZrO₂ for butadiene formation from THF.

Table 1. BET surface area and Brønsted site density of the different catalysts

Catalyst	BET surface area ($m^2\,g^{-1}$)	Brønsted site density[a] ($\mu mol\,g^{-1}$)
H-ZSM-5	425	420
5R WO_x/ZrO_2	58	80
t-ZrO2	84	0
m-ZrO2	20	0
Al_2O_3	120	n.m.
TiO_2	50	n.m.
CeO_2	89	n.m.
Nb_2O_5	10	n.m.

a – Measured by 2-propanamine TPD-TGA

n.m. – not measured

Table 2. Quantification of deactivating species on both zirconia phases

ZrO_2 phase	CO_2 from spent catalyst calcination (μmol g-cat^{-1})	CO_2 adsorption @ 673 K (μmol m^{-2})
Tetragonal	220	0.6
Monoclinic	150	1.0

Zirconia is a highly selective dehydra-decyclization catalyst for the production of diene monomers from biomass derived tetrahydrofurans.

80x37mm (300 x 300 DPI)